Measurement of Myocardial Structure: 3D Structure Tensor Analysis of High Resolution MRI Quantitatively Compared to DT-MRI

Stephen Gilbert[1,3], Mark Trew[4], Bruce Smaill[4], Aleksandra Radjenovic[2], and Olivier Bernus[1,3]

[1] Multidisciplinary Cardiovascular Research Centre
[2] NIHR Leeds Musculoskeletal Biomedical Research Unit University of Leeds, UK
{s.h.gilbert,a.radjenovic,o.bernus}@leeds.ac.uk
[3] L'Institut de ryhtmologie et modélisation cardiaque, Unité Inserm 1045, Centre de Recherche Cardio-Thoracique, Université Bordeaux Segalen, 33076 Bordeaux, France
olivier.bernus@u-bordeaux2.fr
[3]Auckland Bioengineering Institute, The University of Auckland, Auckland, New Zealand
{m.trew,b.smaill}@auckland.ac.nz

Abstract. The ventricular myocardium has a structure of branching laminae through which course regularly orientated fibers, an architecture important in excitation and contraction. DT-MRI is used to measure the fiber and laminar orientations. We quantify the performance of DT-MRI and structure tensor (ST) analysis of 3D high resolution MRI in five rat hearts and validate these against manual measurements. The ST and DT data are more similar for measures of the fiber orientation than laminar orientation. The average angle differences of elevation angles are 2.3±27.2˚, R = 0.57 for the fiber, 3.62±36.2˚, R = 0.24 for the laminae and 10.7±37.9˚, R = 0.32 for the laminae normal. The difference between DT and manually measured laminar orientation is 17±15˚ for DT and 5±10˚ for ST. DT and ST are comparable measures of the fiber orientation but ST is a better measure of myolaminar orientation.

Keywords: myocardium, structure tensor, diffusion tensor, ventricles, small animal imaging, diffusion tensor, structure tensor.

1 Introduction

The mammalian ventricles have a unique and specialized architecture consisting of a regular fiber-orientation which courses through a conserved and complex myolaminar arrangement. Due to the role of these structural features in electrophysiological and biomechanical function in both health and disease, their accurate measure is important. Changes in fiber orientation and myolaminar sliding are thought to be the principle mechanisms of myocardial thickening in systole [1]. Fiber orientation has long been known to influence the spread of myocardial activation [2], and furthermore, laminar organization has recently been shown to substantially influence activation [3]. Myofiber and myolaminar structure are present throughout the myocardium (except in

O. Camara et al. (Eds.): STACOM 2012, LNCS 7746, pp. 207–214, 2013.

the immediate sub-epicardium) and three principal orthogonal structural directions can be defined: (i) along the fiber axis; (ii) perpendicular to the fiber axis in the sheet plane; and (iii) normal to the sheet plane. This structural arrangement is known as orthotropy [3] (Fig. 1).

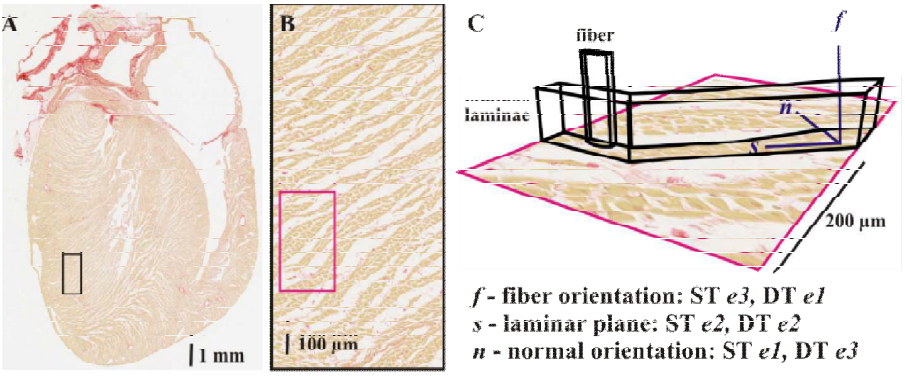

Fig. 1. Cardiac laminar and fiber architecture. (A) coronal long-axis section stained with Picrosirius Red. Cleavage planes – white, myolaminae – rust-red, collagen and fibroblasts – scarlet. (B) magnified region of A. (C) magnified region of B, with a representation of the 3D continuation of myofibers and laminae. The size of a 200 µm voxel is shown and the orientation of the myofibers and myolaminae are labeled, with the corresponding eigenvectors from ST and DT.

Whole-heart computational modeling requires detailed structural atlases [4]. Ideally these would be from accurate high-throughput 3D imaging but current methods have important limitations. 3D histology provides unparalleled spatial-resolution and can be used with molecular labeling but it is only applicable *post mortem* and destroys tissue [5,6]. DT has been widely applied and has been validated for fiber and laminar measurement against 2D methods but it: (i) has limited spatial resolution [7]; (ii) has limited accuracy for laminae [8]; (iii) has not been validated against 3D methods; (iv) is SNR sensitive [7]; (v) the microstructural feature imaged is controversial [9]; and, (vi) the influence of *b*-value has not been fully explored [9]. MicroCT has high spatial-resolution and is fast but has not yet been validated in the myocardium. HR-MRI has high spatial-resolution, is applicable to the beating heart and it has been validated against 2D-histology [10,11]. Structure tensor (ST) analysis is an image analysis method which derives a tensor from the distribution of gradient directions within the neighbourhood of an image voxel [12]. We hypothesized that ST analysis could be applied to HR-MRI images to quantify fiber and laminar orientation, and furthermore that myolaminar orientations from ST would be more accurate and reliable than those from DT as the largest eigenvalue in ST corresponds to the sheet normal direction, whereas in DT the largest eigenvalue corresponds to the fiber direction.

2 Methods

2.1 Heart Preparation and Perfusion Fixation

Male Wistar rats (N = 5) weighing 200 –220 g were euthanized in accordance with the UK Home Office Animals (Scientific Procedures) Act 1986, the hearts were removed and retrograde perfused (as in [11]) with: (i) HEPES-Tyrodes to clear blood; (ii) BDM to prevent contraction; then (iii) MRI contrast agent (0.1% Gd-DTPA) and fixative (4% formaldehyde). Hearts were imaged within 12 hours of fixation.

2.2 HR-MRI and DT-MRI Acquisition and Reconstruction

All hearts were imaged at 20°C using a FLASH (Fast Low Angle SHot) MRI sequence in a Bruker (Ettlingen, Germany) 9.4T spectroscope with 20 averages, echo time (TE) = 7.9 ms, and repetition time (TR) = 50 ms, taking 18h to acquire at a resolution of 50 x 50 x 50 µm. DT was carried out using the same spectroscope on the same hearts with a set of 6 optimized directions using a 3D diffusion-weighted spin-echo sequence with TE = 15 ms, TR = 500 ms, taking 2h to acquire at a resolution of 200 x 200 x 200 µm.

2.3 Structure Tensor Analysis of High Resolution MR Images

A binary mask was created slice-wise from the segmented images by thresholding intensity values and fractional anisotropy and performing a sequence of morphological operations in the following order: clean (removing isolated foreground pixels), bridge (connect pixels separated by one background pixel), fill (fill isolated background pixels), open (binary opening) and a thicken (add pixels around the exterior of an object but do not connect previously unconnected pixels.) Myostructural orientations were computed from the cleaned images by computing intensity gradients with an optimal 5×5×5 point derivative template [13]. The template was applied to the full 3D image using 1D FFT convolution. The structure tensor (the outer product of the intensity gradient vectors) was computed for each voxel in the 3D image. A sequence of structure tensors at progressive resolution doubling (i.e. 100 µm, 200 µm, 400 µm, etc.) was determined using a level 4 binomial filter. These calculations are completed in around 1 minute. The 200 µm smoothed structure tensor data set (64×64×128 tensors) was used to best match the expected DT resolution. Eigenanalysis was used to extract the principal directions from the structure tensor at each discrete point (the calculation requires < 10 s). The eigenvector corresponding to the largest magnitude eigenvalue was taken as the sheet/laminae normal direction and the eigenvector corresponding to the smallest magnitude eigenvalue was taken as the fiber direction (Fig. 1).

2.4 Comparison of Structure Tensor and Diffusion Tensor Orientations

A model cardiac geometry, with a manually fitted LV long-axis, was registered to each heart MRI by affine registration (using the Insight Tool Kit fast affine registration

implemented in Slicer3) with 20 histogram bins, 40000 spatial samples and 4000 iterations. The registered model hence defines: (i) the long-axis (LA) centroid of a cylindrical coordinate system for which the elevation and azimuth angles of the eigenvectors were calculated. and, (ii) selected regions of interest (ROI) for quantification. The orientation angles reported are defined in detail in [14]. Elevation angles are measured from the cardiac short-axis (SA) plane. The fiber helix angle (α_H) is the angle between the transverse plane and the projection of the fiber vector onto the circumferential-longitudinal plane. The fiber transverse angle (α_T) is the angle between the circumferential-longitudinal plane and the projection of the fiber vector onto the transverse plane. The angle between the transverse plane and the projection of the laminar vector onto the radial-longitudinal plane *is* B'_S. The angle between the longitudinal—radial plane and the projection of the laminar vector onto the transverse plane B''_S. The angles B'_N and B''_N correspond to B'_S and B''_S but are the orientations of the normal of the laminar plane. A mid-heart coronal long-axis plane was selected for visualization and quantification, and within this a ROI measuring 5.1 x 5.1 mm was selected and ST and DT B'_S was visualised. ST and DT B'_S was compared to manually measured laminar orientation in a 1.1 x 1.1 mm sub-region, by using ImageJ to measure orientation in 200 µm grid squares in the HR-MRI data.

3 Results

Fig. 2 shows unprocessed HR-MRI SA and LA images and alongside these are LA β' and α_H maps and SA α_H and α_T maps. As previously demonstrated [10,11] the laminar organization can be clearly observed in the HR-MRI images. The α_H and α_T maps show that the values and spatial distribution of the fiber orientation measured by ST and DT is strikingly close. The β' maps reveal related values with some differences between the ST and DT determined sheet elevation angle. These differences are in regions where the myocardium is compact and cleavage planes difficult to discern. The angle distributions (Fig. 2E&F) reflect these observations.

The ST and DT determined orientations were compared in the selected equatorial SA slice (Table 1). The mean angle differences are low for the fiber orientation angles (2.3° for α_H, 1.7° for α_T) and there is good correlation between the ST and DT α_H (circular correlation coefficient R = 0.57). The correlation of ST and DT α_T is weaker (R = 0.29). The average angle difference and correlation coefficients for the sheet orientation measures are likewise weaker but all correlations are significant.

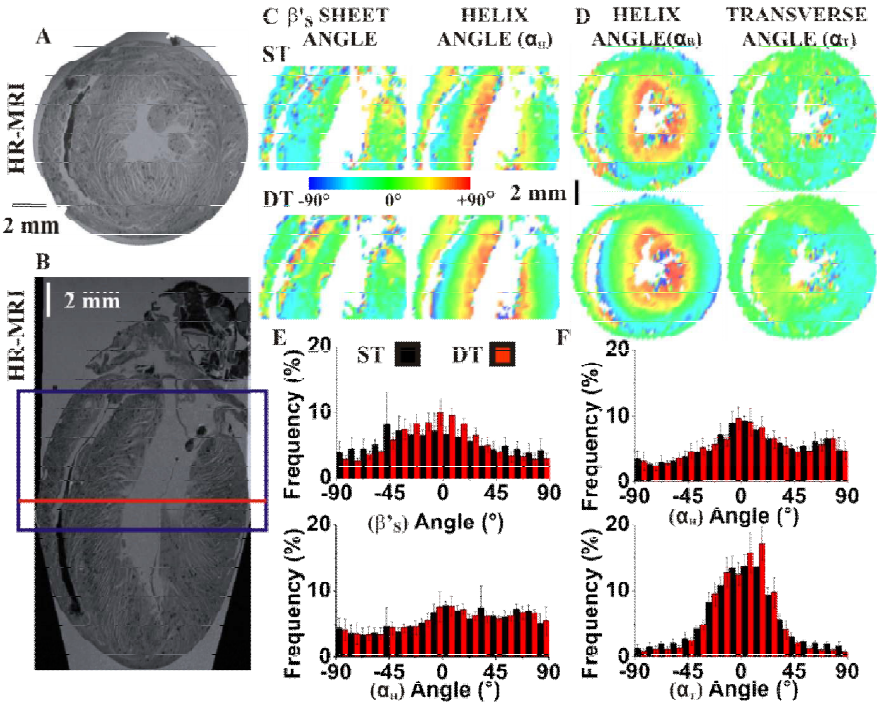

Fig. 2. Visualization of DT and ST α_H, α_T and β' maps and associated angle distributions. (**A**) SA HR-MRI image of ROI. (**B**) LA HR-MRI image, with the LA ROI highlighted in the blue box and the SA ROI highlighted by the red line. (**C**) LA β_S' and α_H for ST (top panel) and DT (lower panel). (**D**) SA α_H and α_T for ST (top panel) and DT (lower panel). (**E**) Angle distributions corresponding to images in LA maps, β'_S upper panel, α_H bottom panel. (**F**) Angle distributions corresponding to images in SA maps, α_H – upper panel, α_T bottom panel.

Table 1. The average difference (*mean* **Δ**) angles pooled the selected equatorial slice in the five hearts. * - correlation statistically significant at $p < 0.05$.

		α^H	α^T	β'_S	β''_S	β'_N	β''_N
mean Δ	***x***	2.3	1.7	3.6	4.8	10.7	6.4
	σ	27.2	29.1	36.2	36.0	37.9	35.2
corr.	***R***	0.57*	0.29*	0.24*	0.24*	0.32*	0.34*

Fig. 3 compares the performance of DT and ST against manual measurement from HR-MRI. The magnified regions in Fig. 3E&F allow the visual assessment of the performance of ST and DT. In regions where the laminae are clearly defined by cleavage planes ST performs better than DT. It is not possible to assess the performance of the methods in the regions where laminar structure is not clearly defined (such as Fig 3E, top left of image).

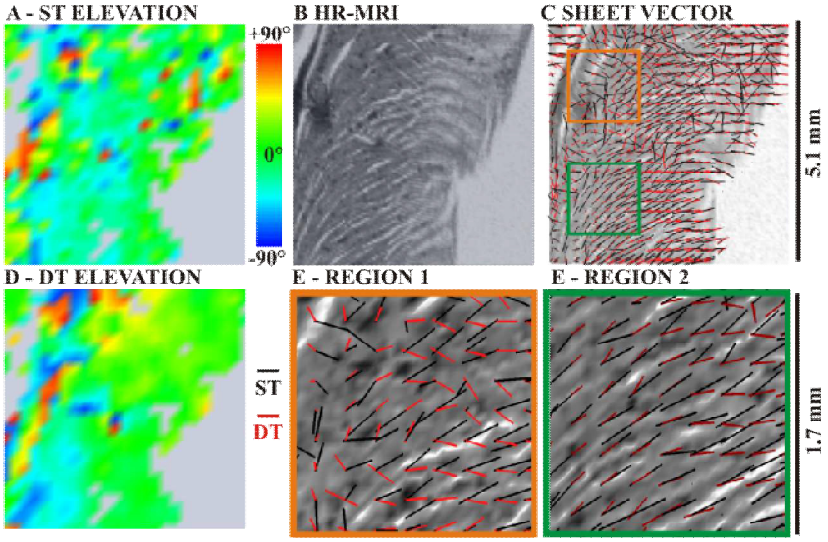

Fig. 3. Quantitative validation of DT and ST against manual measurements of sheet elevation angle (β') in HR-MRI images. A region was selected from the LA ROI in Fig. 2. (**A**) ST β' map. (**B**) The HR-MRI of the ROI. (**C**) The 3D orientation of the sheet vector within individual voxels in the ROI is shown by line glyphs, black for ST, red for DT. (**D**) DT β' map. (**E**) magnified orange box from panel B. (**F**) magnified green box from panel B.

Laminar elevation in the ROI in Fig. 3F was manually measured and the angle difference between the manual measurements (mean ± standard deviation) is 17±15° for DT and 5±10° for ST.

4 Discussion

DT and ST produce similar maps of fiber orientation. The maps of laminar orientation from DT and ST are related but ST is a consistently more acceptable measure, as shown by both visual comparison and by manual measurements. We demonstrate that the distinct approaches of DT and of ST produce globally and locally similar maps of fiber orientation. Although fiber orientation measurement by ST of myocardial images has been proposed [15] this is the first whole heart demonstration of the method. The quality of the ST α_H and α_T maps and the similarity to the DT maps is striking, particularly as the HR-MRI spatial resolution is not high enough to allow the manual identification of myocytes. Indeed, due to this resolution limitation it is not possible to directly validate DT or ST against manual measurements of fiber orientation from the HR-MRI data. DT and ST produce maps of laminar orientation which share some similarities, but there are also regions of marked difference. We show that the average difference between manual and DT β' measurement is 17±15°, while it is only 5±10° for ST β' measurement in a selected ROI. On this basis we propose that ST of HR-MRI is a useful method for measurement of whole heart laminar orientation and

performs superiorly to DT. Based on our data, DT provides limited accuracy when assessed in myocardium with easily discernible laminae and cleavage plane directions. An important question for the choice of method used to measure laminar orientation is the degree of accuracy required. Until recently the histological validation of DT in the measurement of laminar orientation has been small scale and 2D [16] or using an unconventional 2D ink-blot approach [17]. In a recent study the difference between histologically and DT determined sheet angles was reported as 8° ± 27° and the authors concluded that the measurement of myolaminae by the DT corresponds to histology [8]. Therefore, [8] reported a better performance of DT (albeit with high standard deviation) than we found. This is particularly of note as in [8] DT was assessed against histology and we assessed DT against HR-MRI. The accuracy of DT claimed by [8] is strikingly positive, particularly considering the substantial distortion of tissue, which accompanies sectional histological laminar orientation. It is our view that DT can be much more reliably assessed against the volumetric HR-MRI method as the same tissue preparation is sequentially imaged in the MRI scanner with no myocardial distortion or damage. There are some limitations in this preliminary study. It is possible that greater numbers of diffusion directions, greater numbers of repetitions, alternative b-values or alternative voxel sizes may increase the accuracy of DT applied to the myocardium, and a detailed sensitivity analysis has not yet been reported. In this study we assess the performance of 6 directions DT, but recent evidence suggests that this has comparable robustness to 30- or 60-direction data [18]. Future studies will incorporate sensitivity analysis of both ST and DT.

References

1. Costa, K.D., Takayama, Y., McCulloch, A.D., Covell, J.W.: Laminar fiber architecture and three-dimensional systolic mechanics in canine ventricular myocardium. Am. J. Physiol. 276, H595–H607 (1999)
2. Arisi, G., Macchi, E., Baruffi, S., Spaggiari, S., Taccardi, B.: Potential fields on the ventricular surface of the exposed dog heart during normal excitation. Circ. Res. 52, 706–715 (1983)
3. Hooks, D.A., Trew, M.L., Caldwell, B.J., Sands, G.B., LeGrice, I.J., Smaill, B.H.: Laminar arrangement of ventricular myocytes influences electrical behavior of the heart. Circ. Res. 101, 103–112 (2007)
4. Sermesant, M., Chabiniok, R., Chinchapatnam, P., Mansi, T., Billet, F., Moireau, P., Peyrat, J.M., Wong, K., Relan, J., Rhode, K., Ginks, M., Lambiase, P., Delingette, H., Sorine, M., Rinaldi, C.A., Chapelle, D., Razavi, R., Ayache, N.: Patient-specific electromechanical models of the heart for the prediction of pacing acute effects in CRT: a preliminary clinical validation. Med. Image. Anal. 16, 201–215 (2012)
5. Sands, G.B., Gerneke, D.A., Hooks, D.A., Green, C.R., Smaill, B.H., LeGrice, I.J.: Automated imaging of extended tissue volumes using confocal microscopy. Microsc. Res. Tech. 67, 227–239 (2005)
6. Smith, R.M., Matiukas, A., Zemlin, C.W., Pertsov, A.M.: Nondestructive optical determination of fiber organization in intact myocardial wall. Microsc. Res. Tech. 71, 510–516 (2008)

7. Jiang, Y., Pandya, K., Smithies, O., Hsu, E.W.: Three-dimensional diffusion tensor microscopy of fixed mouse hearts. Magn. Reson. Med. 52, 453–460 (2004)
8. Kung, G.L., Nguyen, T.C., Itoh, A., Skare, S., Ingels Jr., N.B., Miller, D.C., Ennis, D.B.: The presence of two local myocardial sheet populations confirmed by diffusion tensor MRI and histological validation. J. Magn. Reson. Imaging 34, 1080–1091 (2011)
9. Hsu, E.W., Buckley, D.L., Bui, J.D., Blackband, S.J., Forder, J.R.: Two-component diffusion tensor MRI of isolated perfused hearts. Magn. Reson. Med. 45, 1039–1045 (2001)
10. Köhler, S., Hiller, K.H., Waller, C., Jakob, P.M., Bauer, W.R., Haase, A.: Visualization of myocardial microstructure using high-resolution T*2 imaging at high magnetic field. Magn. Reson. Med. 49, 371–375 (2003)
11. Gilbert, S.H., Benoist, D., Benson, A.P., White, E., Tanner, S.F., Holden, A.V., Dobrzynski, H., Bernus, O., Radjenovic, A.: Visualization and quantification of whole rat heart laminar structure using high-spatial resolution contrast-enhanced MRI. Am. J. Physiol. Heart. Circ. Physiol. 302, H287–H298 (2012)
12. Jähne, B.: Digital image processing, 6th edn. Springer, The Netherlands (2005)
13. Farid, H., Simoncelli, E.P.: Differentiation of discrete multidimensional signals. IEEE Trans. Image Process. 13, 496–508 (2004)
14. Benson, A.P., Gilbert, S.H., Li, P., Newton, S.M., Holden, A.V.: Reconstruction and Quantification of Diffusion Tensor Imaging-Derived Cardiac Fibre and Sheet Structure in Ventricular Regions used in Studies of Excitation Propagation. Math. Model. Nat. Pheno. 3, 101–130 (2008)
15. Burton, R.A., Plank, G., Schneider, J.E., Grau, V., Ahammer, H., Keeling, S.L., Lee, J., Smith, N.P., Gavaghan, D., Trayanova, N., Kohl, P.: Three-dimensional models of individual cardiac histoanatomy: tools and challenges. Ann. N. Y. Acad. Sci. 080, 301–319 (2006)
16. Scollan, D.F., Holmes, A., Winslow, R., Forder, J.: Histological validation of myocardial microstructure obtained from diffusion tensor magnetic resonance imaging. Am. J. Physiol. 275, H2308–H2318 (1998)
17. Tseng, W.Y., Wedeen, V.J., Reese, T.G., Smith, R.N., Halpern, E.F.: Diffusion tensor MRI of myocardial fibers and sheets: correspondence with visible cut-face texture. J. Magn. Reson. Imaging 17, 31–42 (2003)
18. Lebel, C., Benner, T., Beaulieu, C.: Six is enough? Comparison of diffusion parameters measured using six or more diffusion-encoding gradient directions with deterministic tractography. Magn. Reson. Med. (2011) (in press)